ChemComm

Accepted Manuscript

This is an *Accepted Manuscript*, which has been through the Royal Society of Chemistry peer review process and has been accepted for publication.

Accepted Manuscripts are published online shortly after acceptance, before technical editing, formatting and proof reading. Using this free service, authors can make their results available to the community, in citable form, before we publish the edited article. We will replace this *Accepted Manuscript* with the edited and formatted *Advance Article* as soon as it is available.

You can find more information about *Accepted Manuscripts* in the **Information for Authors**.

Please note that technical editing may introduce minor changes to the text and/or graphics, which may alter content. The journal's standard **Terms & Conditions** and the **Ethical guidelines** still apply. In no event shall the Royal Society of Chemistry be held responsible for any errors or omissions in this *Accepted Manuscript* or any consequences arising from the use of any information it contains.

ChemComm

Dynamic Article Links ▶

COMMUNICATIONS

High-sensitivity fluorescence imaging of iron in plant tissues

Mi-Jeong Park,[a,c] Hak-Sung Jung,[a,c] Young-Jae Kim,[a] Young-Ju Kwon,[a] Jin-Kyu Lee*[a] and Chung-Mo Park*[a,b]

Here, we report a method for high-sensitivity fluorescence imaging of iron, which demonstrates the abundance and distribution of iron in plant tissues more precisely than conventional histochemical staining procedures. The fluorescence turn-on method is rapid (< 20 min), inexpensive to set up, and expected to be readily applicable to any plant tissues.

Iron is a vital micronutrient that plays a critical role in a wide range of fundamental biological reactions in plants, such as electron transport chains in photosynthesis, respiration, cell division, and nitrogen fixation.[1] The versatile roles of iron arise from its chemical property: it exists in two alternative oxidation states, ferric ion (Fe^{3+}) and ferrous ion (Fe^{2+}). However, the dual oxidation characteristic of iron potentiates oxygen toxicity by generating reactive oxygen species, which cause oxidative damage to biomolecules. Therefore, plants tightly maintain iron homeostasis through coordinated regulation of its uptake, transport, and storage.[2]

The physiological roles of iron have been explored by molecular genetic and biochemical studies of mutant plants exhibiting defects in iron metabolism and by measurements of iron contents via inductively coupled plasma mass spectrometry.[3] In recent years, there has been a growing concern for high-resolution imaging of iron distribution in plant tissues, which is a prerequisite for understanding the dynamic iron metabolic processes in plant growth and development and environmental stress responses. X-ray fluorescence microtomography and electron microscopy coupled to inelastically scattered electrons have been adopted for investigating the specific localization of iron in plants.[4,5] However, because of technical difficulties associated with these methods, histochemical staining methods, such as Perls staining,[6] are still routinely used. Although the Perls staining method has been improved,[7-9] a major sink of iron in plants, the leaves, is poorly stained by histochemical methods, and the resolution of iron detection remains poor. The experimental procedures involved are also complex and time-consuming.

An array of fluorescent probes has been developed for imaging of diverse biomolecules in plants and animals. Unlike absorbance-based probes for iron detection, such as the blue precipitate of Perls staining and the black precipitate of DAB-intensified Perls (Perls/DAB) staining, fluorescence-based sensors are highly sensitive, providing nearly infinite contrast by emitting light on a dark background. In addition to visualization of specific biomolecules with high sensitivity, detection by fluorescent probes is simple, precise, and quantitative. Recently, several fluorescent probes have been synthesized for the detection of iron in cells.[10-14] However, these have not yet been tested for their application in plant tissues.

When considering fluorescent probes that may be appropriate for selective detection of iron in plant tissues, we chose MPNBD (7-(4-methylpiperazin-1-yl)-4-nitrobenz-2-oxa-1,3-diazole) as a photoinduced electron transfer (PET) fluoroionophore for the evaluation of its potential application in plants (Scheme 1),[10,15,16] based on the following reasons. First, MPNBD displays high fluorescence enhancement in the presence of physiological concentrations of Fe^{3+} with low background emission. Second, chelation of Fe^{3+} by MPNBD induces emission in the green region, which is easily distinguishable from red autofluorescence in plants. In addition, it is efficiently excited by wavelengths above 430 nm, thus avoiding cellular and tissue damage.
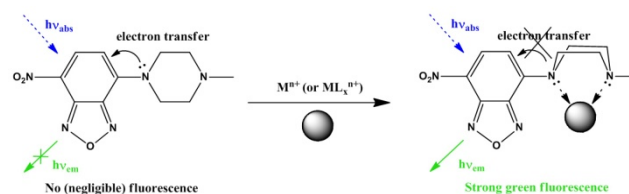
Scheme 1. Chemical structure of MPNBD and its photoinduced electron transfer (PET) fluoroionophore mechanism. M, metal ion; n, oxidation number; L, solvent or other ligand molecule.

We synthesized MPNBD according to a previously described procedure,[10] and the purity and structural integrity of the synthesized MPNBD were verified by NMR spectra and mass spectrometry (Fig. S1-S3, ESI†). To establish proper detection conditions, we investigated the absorption and emission spectra of MPNBD in water and ethanol, along with the various amounts of Fe^{3+}. In ethanol, MPNBD showed a higher fluorescence response to Fe^{3+} in comparison to that observed for MPNBD in water (Fig. S4, ESI†), supporting the relevance of ethanol as the solvent of choice for MPNBD. It is well known that ethanol is compatible with most histological assays on plant tissues. We therefore decided to adopt the ethanol-based detection condition in our assays.

We examined fluorescence responses of MPNBD to various metal ions in ethanol, including Fe^{3+} and Fe^{2+} (Fig. 1 and Fig. S5-S8, ESI†). Notably, treatments with Fe^{3+} and Fe^{2+} induced

obvious fluorescence turn-on responses at 533 nm (Fig. 1). MPNBD showed different fluorescence responses to Fe^{3+} and
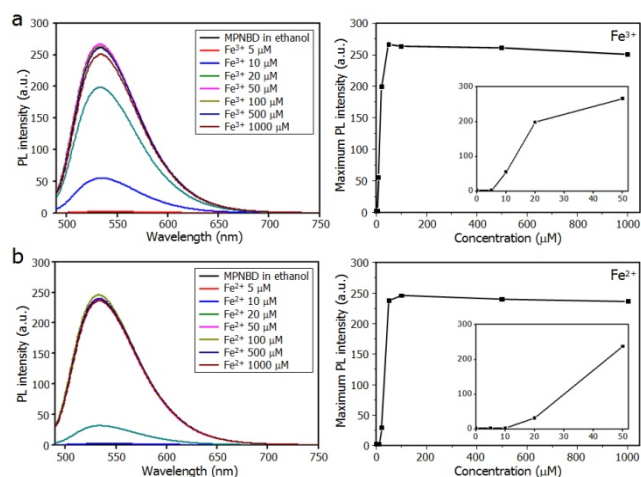

Figure 1. Fluorescence response of MPNBD to Fe^{3+} (a) and Fe^{2+} (b) ions. Different concentrations of iron ions were added to MPNBD solution in ethanol, and the mixtures were subject to UV-vis spectroscopy and fluorophotometry. Fluorescence spectra under the irradiation at 470 nm are shown in the left panels. Plots of maximum photoluminescence (PL) emission intensity at 533 nm are shown in the right panels. The insets show plots of maximum PL intensities in the concentration range of 0 to 50 μM for Fe^{3+} or Fe^{2+}. a.u., arbitrary unit.

Fe^{2+}, depending on the concentration of ions. The emission intensity induced by Fe^{3+} was higher by approximately 6-fold than that induced by Fe^{2+} at low concentrations (<50 μM) (see Insets in Figure 1). In contrast, the emission intensities of Fe^{3+} and Fe^{2+} were similar at high concentrations (>50 μM) (Figure 1).

The fluorescence signals enhanced by Fe^{3+} and Fe^{2+} were much higher than those enhanced by other metal ions that are plentiful in plants, such as K^+, Ca^{2+} and Mg^{2+} (Fig. S7c and S8, ESI†), suggesting that MPNBD is useful as a fluorescence probe for detection of iron ions in plants. The detection limit of MPNBD for Fe^{3+} was determined to be 8.08 μM (Fig. S9, ESI†), which is much lower than the detection limit of conventional histochemical staining methods.

We found that 50 μM Cr^{3+} elicited approximately half of the emission intensity by iron (Fig. S7a, ESI†). Since the concentration of Cr^{3+} is extremely low in plants, the fluorescence enrichment by Cr^{3+} would essentially be negligible in measuring the fluorescence enrichment of MPNBD by Fe^{3+} and Fe^{2+}. Fifty μM Cu^{2+} induced less than 1% of the emission intensity by iron (Fig. S7b, ESI†). Based on these results together with the relatively low concentration of Cu^{2+} compared to that of iron in plants, we reasoned that endogenous Cu^{2+} does not distort the sensing of iron by MPNBD.

To further evaluate the specific sensing of Fe^{3+} by MPNBD, we performed competition experiments by including other metal ions in the assays. The fluorescence intensities of the mixtures of Fe^{3+} and other metal ions were similar to that by Fe^{3+} alone (Fig. S10, ESI†). It was therefore concluded that the fluorescent turn-on probe MPNBD is suitable for the selective imaging of iron in plant tissues.

We next examined the validity of MPNBD as a fluorescent probe for the imaging of iron distribution in plants using the dicot model *Arabidopsis thaliana*. The *Arabidopsis* seedlings soaked in

50 μM MPNBD solution were subject to vacuum infiltration (ESI†). The seedlings were then incubated in complete darkness and washed with ethanol before fluorescence microscopy. The Perls and Perls/DAB staining methods were also conducted in parallel for comparative analysis using the *Arabidopsis* seedlings of the same age (Fig. 2).

Significantly high fluorescence signals were reproducibly observed in the *Arabidopsis* plants treated with MPNBD (Fig. S11, ESI†). However, no detectable signals were observed in mock-treated plants, indicating that autofluorescence does not interfere with the MPNBD-mediated fluorescence emission in plants. We also found that the MPNBD probe is relatively stable. The fluorescent signals did not significantly diminish even after 3 h (Fig. S12, ESI†). In addition, the presence of other metal ions did not detectably interfere with the sensing of iron by MPNBD *in planta* (Fig. S13, ESI†). We did not include Cr^{3+} in the assays. Although MPNBD showed certain amount of fluorescence response to this metal ion (Fig. S7a, ESI†), its concentration is extremely low in plants.

The Perls staining gave signals primarily in the root tissues. However, it failed to detect discernible signals in the aerial plant parts, as reported previously.[17] The improved Perls/DAB staining produced signals from both the roots and aerial plant parts. However, it suffered from low resolution, as this detection method is based on black precipitates. Notably, the MBNBD-based fluorescence turn-on assays exhibited high fluorescence signals throughout all plant organs, including the leaves, within 20 min following MPNBD treatments (Fig. 2).
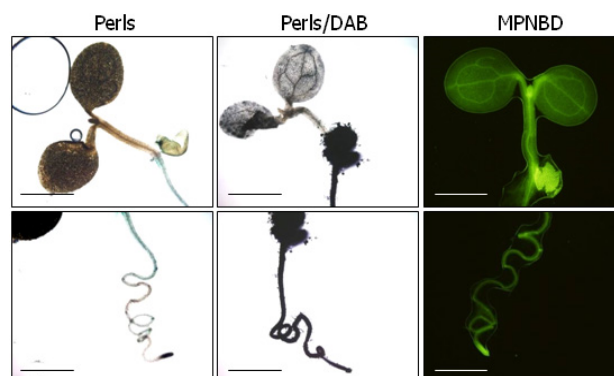

Figure 2. Comparison of different iron detection methods in plants. Four-day-old whole *Arabidopsis* seedlings grown on 1/2 X Murashige & Skoog (MS) media containing 0.6% (w/v) agar (hereafter referred to as MS-agar plates) were subject to different iron detection methods as described in Table S1. The aerial plant parts are shown in the top panels, and the roots are shown in the bottom panels. Scale bars, 0.5 cm.

A prominent feature of the MPNBD-based fluorescence detection method is the high-resolution imaging of iron distribution in plants. It successfully visualized iron distribution in different plant tissues with subcellular resolution (Fig. 2, see below). The localized distribution of iron in the leaf tissues is controversial. It has been reported that approximately 70% of the total iron measured in the leaves is found in the chloroplasts.[18] On the other hand, a considerable amount of iron has also been detected in the vasculature of the leaves.[19] The MPNBD fluorescence method visualized high-resolution signals in both the chloroplasts and vasculature of the leaves (Fig. 3a and Fig. 2, respectively), demonstrating that iron accumulates in both the

chloroplasts and vasculature of the leaves. There was also high-level fluorescence emission in the vasculature of the stems and roots after MPNBD treatments (Fig. 3b and Fig 3c,d, respectively). Moreover, the MPNBD-assisted high-resolution imaging revealed that iron accumulates at a high level in the epidermal cells of the seed coat (Fig. 3e), especially in the volcano-shaped columella and hexagonal cell wall (Fig. 3f). It has been reported that Ca^{2+} is deposited in a similar pattern in the seed coat.[20] We therefore suspected that the fluorescence emission might be from MPNBD-Ca^{2+} complex. However, the fluorescence enrichment of MPNBD by Ca^{2+} was beyond the detection limit of our assay conditions (Fig. S7c, ESI†), indicating that fluorescence emission in the seed coat was due to iron deposits. Nonetheless, the biological function of iron deposited in the seed coat is currently unknown.
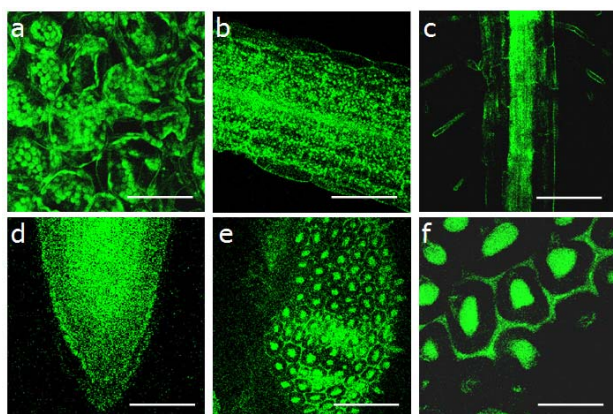

Figure 3. Fluorescence images of plants treated with MPNBD. Four-day-old, whole *Arabidopsis* seedlings grown on MS-agar plates were treated with 50 μM MPNBD and visualized by fluorescence microscopy. (**a**) Fluorescence image of leaf epidermal cells. Scale bar, 60 μm. (**b**) Fluorescence image of the stem. Scale bar, 120 μm. (**c** and **d**) Fluorescence image of the root stem (**c**) and the root tip region (**d**). Scale bars, 110 μm (**c**) and 60 μm (**d**). (**e** and **f**) Fluorescence images of developing seed. *Arabidopsis* seed were cold-imbibed for 3 days in complete darkness and allowed to germinate for 12 hours before MPNBD treatments. An enlarged view (**f**) of the developing seed (**e**) was shown. Scale bars, 110 μm (**e**) and 40 μm (**f**).

Our data demonstrate that the fluorescence turn-on probe MPNBD is able to image the distribution of total iron in all plant tissues with high resolution and high sensitivity (Table S1, ESI†). In addition, the MPNBD-assisted fluorescence detection method can be readily applied to all plant organs with a simple procedure and low cost. Furthermore, due to the high binding affinity of MPNBD to iron, it is unnecessary to treat plant samples with acids to release iron from iron complexes prior to MPNBD treatment. Since the MPNBD method is based on fluorescence emission, sectioning of plants tissues is not necessary for small plants, such as *Arabidopsis*.

Conclusions

In conclusion, the MPNBD fluorescence method provides high-resolution imaging of total iron in plant tissues. Therefore, dynamic information on the redox chemistry of iron can be obtained if it is applied in conjunction with Fe^{3+}- and Fe^{2+}-specific fluorescent probes. This method is potentially useful for the isolation of mutant plants that are defective in iron

metabolism and deposit in a high-throughput manner.

Notes and references

a Department of Chemistry, Seoul National University, Seoul 151-742, Korea. Fax: +82-2-882-1080; E-mail: jinklee@snu.ac
b Plant Genomics and Breeding Institute, Seoul National University, Seoul 151-742, Korea. Fax: +82-2-886-6697; E-mail: cmpark@snu.ac.kr
c These authors contributed equally to this work.
† Electronic Supplementary Information (ESI) available: Detailed experimental procedures, the ^{1}H-, ^{13}C-NMR, and MS spectra, supplementary spectra, and comparison of different iron staining procedures, etc. See DOI: 10.1039/b000000x/

1   J.F. Briat, C. Curie and F. Gaymard, *Curr. Opin. Plant Biol.*, 2007, **10**, 276.
2   J. Jeong and M.L. Guerinot, *Trends Plant Sci.*, 2009, **14**, 280.
3   T.A. Long, H. Tsukagoshi, W. Busch, B. Lahner, D.E. Salt and P.N. Benfey, *Plant Cell*, **2010**, 22, 2219.
4   S.A. Kim, T. Punshon, A. Lanzirotti, L. Li, J.M. Alonso, J.R. Ecker, J. Kaplan and M.L. Guerinot, *Science*, 2006, **314**, 1295.
5   V. Lanquar, F. Lelièvre, S. Bolte, C. Hamès, C. Alcon, D. Neumann, G. Vansuyt, C. Curie, A. Schröder, U. Krämer, H. Barbier-Brygoo and S. Thomine, *EMBO J.*, 2005, **24**, 4041.
6   P.J. Seo, J. Park, M.J. Park, Y.S. Kim, S.G. Kim, J.H. Jung and C.M. Park, *Biochem. J.*, 2012, **442**, 551.
7   H. Roschzttardtz, G. Conéjéro, C. Curie and S. Mari, *Plant Physiol.*, 2009, **151**, 1329.
8   H. Roschzttardtz, G. Conéjéro, F. Divol, C. Alcon, J.L. Verdeil, C. Curie and S. Mari, *Front. Plant Sci.*, 2013, **4**, 350.
9   M. Bournier, N. Tissot, S. Mari, J. Boucherez, E. Lacombe, J.F. Briat and F. Gaymard, *J. Biol. Chem.*, 2013, **288**, 22670.
10 Y. Xiao and X. Qian, *Tetrahedron Lett.*, 2003, **44**, 2087.
11 S.R. Liu and S.P. Wu, *Sensor. Actuat. B-Chem.*, 2012, **171-172**, 1110.
12 S.K. Sahoo, D. Sharma, R.K. Bera, G. Crisponi and J.F. Callan, *Chem. Soc. Rev.*, 2012, **41**, 7195.
13 S. Goswami, K. Aich, S. Das, A.K. Das, D. Sarkar, S. Panja, T.K. Mondal and S. Mukhopadhyay, *Chem. Comm.*, 2013, **49**, 10739.
14 T. Hirayama, K. Okuda and H. Nagasawa, *Chem. Sci.*, 2013, **4**, 1250.
15 B. Ramachandram and A. Samanta, *J. Phys. Chem. A*, 1998, **102**, 10579.
16 T. Mistri, R. Alam, M. Dolai, S.K. Mandal, A.R. Khuda-Bukhsh and M. Ali, *Org. Biomol. Chem.*, 2013, **11**, 1563.
17 L.S. Green and E.E. Rogers, *Plant Physiol.*, 2004, **136**, 2523.
18 T. Shikanai, P. Muller-Moule, Y. Munekage, K.K. Niyogi and M. Pilon, *Plant Cell*, 2003, **15**, 1333.
19 M.G. Stacey, A. Patel, W.E. McClain, M. Mathieu, M. Remley, E.E. Rogers, W. Gassmann, D.G. Blevins and G. Stacey, *Plant Physiol.*, 2008, **146**, 589.
20 C. Voiniciuc, G.H. Dean, J.S. Griffiths, K. Kirchsteiger, Y.T. Hwang, A. Gillett, G. Dow, T.L. Western, M. Estelle and G.W. Haughn, *Plant Cell*, 2013, **25**, 944.